

Graphene-based midinfrared photodetector with bull's eye plasmonic antenna

Xiangying Deng^{a,b,*}, Shunri Oda,^a and Yukio Kawano^{a,c,d}

^aTokyo Institute of Technology, Department of Electrical and Electronic Engineering, Tokyo, Japan

^bWestern Digital Technologies, Inc., Milpitas, California, United States

^cNational Institute of Informatics, Tokyo, Japan

^dChuo University, Department of Electrical, Electronic, and Communication Engineering, Faculty of Science and Engineering, Tokyo, Japan

ABSTRACT. The spectral region of midinfrared has proven its great potential in various fields, such as materials characterization, medical examination, security, and product inspection. However, the development of room-temperature sensitive midinfrared photodetectors is inevitably in strong demand. Graphene-based detectors are expected to potentially overcome many of the shortcomings of earlier detectors. Unfortunately, low light absorption originating from a single atomic layer is still an obstacle for sensitive sensing using graphene-based photodetectors. To optimize the performance of plasmonic antenna, we have proposed wideband bull's-eye-shaped antennas using cavity-mode resonance for the midinfrared region. The proposed multi-resonant frequency plasmonic antennas are integrated with graphene-based detectors for midinfrared detection. We demonstrated that the graphene device integrated with the multifrequency plasmonic antenna enabled the room-temperature sensitive midinfrared detection. In addition, such a device can achieve frequency filtering measurement through the bull's eye shaped plasmonic antenna. The coupling of antenna onto the device largely spares the integration space. We believe that such a device is practical in various applications that require room-temperature, frequency selective sensitive photo detection.

© The Authors. Published by SPIE under a Creative Commons Attribution 4.0 International License. Distribution or reproduction of this work in whole or in part requires full attribution of the original publication, including its DOI. [DOI: [10.1117/1.OE.62.9.097102](https://doi.org/10.1117/1.OE.62.9.097102)]

Keywords: graphene; midinfrared; photodetector; plasmonic antenna

Paper 20230429G received May 6, 2023; revised Jul. 26, 2023; accepted Aug. 18, 2023; published Sep. 8, 2023.

1 Introduction

The midinfrared light has been promising for a variety of applications including security, product inspection, material analysis, and thermal analysis. This region has been attracting many researchers and has long been studied as it relates to most of thermal radiation and molecular vibrations. Among those studies, room temperature, sensitive midinfrared photodetectors are in strong demand to fulfill the many significant applications of midinfrared spectrum. Existing midinfrared detectors, such as high-electron-mobility transistors, field effect transistors, and Si-MOSFET, use techniques such as heterojunction structures and gate modulation of a conductance channel.^{1,2} Certain shortcomings of these techniques include high production prices, complexity, and low detection rate. Graphene is one of the two-dimensional materials and has attracted a lot of attention recently, which are expected to overcome many of these problems. It can absorb and convert light into photocurrent due to its zero band gap, high carrier mobility, and electron-hole symmetry. In addition, graphene was shown to work as sensitive high-speed

*Address all correspondence to Xiangying Deng, dengxiangying77@gmail.com

photodetectors for a wide range of electromagnetic spectrum under room temperature.^{3–10} Furthermore, graphene can be fabricated at low cost by either mechanical exfoliation or chemical vapor deposition (CVD). Especially, when using CVD for graphene fabrication, we can get large-scale and high quality graphene sheets.

However, there is still plenty of room for graphene-based infrared detectors to enhance performance in light-coupling efficiency. Among the various methods that have been made to enhance the responsivity of graphene photodetectors, combining metallic subwavelength plasmonic antennas directly onto the graphene is one of the promising approaches.^{11–26} These plasmonic metal-based antennas can localize plasmonic polaritons and cause strong field enhancement when illuminated by electromagnetic signal. These enhancements can be guided to the nanoscale gaps with graphene covered nearby and significantly enhance the light–matter interaction. Plasmon be guiding along the interface between the dielectric and metal in the form of a traveling wave is called surface plasmon polariton (SPP). Though some researchers argue that in the THz region there might be no SPPs, spoof plasmons (SPs) that mimic SPPs have similar electromagnetic characteristics and were proved to exist in the midinfrared region.²⁷ Bull's eye antenna is one of the plasmonic structures that can achieve such purpose. A bull's eye structure consists of a single subwavelength aperture in the middle. Outside the aperture are concentric periodic grooves. When the periodic grooves are fitted to the designed frequency, it can generate the SPPs at the interface and guide the SPPs toward the aperture. Then, a highly enhanced and concentrated electric field appears at the sub-wavelength aperture due to the Bragg condition. Because of its significant advantages, bull's eye structures have been studied in a wide frequency region.^{28–36} Despite the many advantages of conventional bull's eye antennas, there still exists a main limitation for the bull's eye shaped plasmonic antenna, which is its single-resonant frequency. The single resonant frequency of bull's eye antenna has limited its usefulness in various applications that requires frequency tunable spectroscopy and imaging. Thus, essential improvements regarding its bandwidth are still in urgent demand.

2 Wideband Plasmonic Antenna Coupled Graphene Photodetector Design

In this paper, we use one complete bull's eye plasmonic antenna to cover the whole graphene ribbon, leaving only an aperture that allows midinfrared irradiation to transmit through. The graphene will be connected to the electric circuit with two ordinary electrodes. In this design, the aperture is located at the interception between the graphene ribbon and one of its electrodes. The heated side will thus have a higher temperature than the other side, causing a thermoelectric signal through Seebeck effect. To reduce the fabrication expenses, Ni is used as electrode material for graphene ribbons. Al is used as the fabrication material for bull's eye antenna. Since the electrode and the plasmonic antenna are both conductive, in order to prevent short circuit, we grew a 70 nm of Al₂O₃ in between the plasmonic antenna and the graphene device structure. Figure 1 exhibits our device design for the full-BE coupled graphene based midinfrared detector.

FDTD simulations on plasmonic antennas were performed before fabrication of the device. The simulation of bull's eye structure is conducted using a three-dimensional finite difference time domain method software (Poynting of optics, Fujitsu, Co., Japan). Due to the single resonance frequency nature of a conventional BE antenna, its parameters depend on the desired frequency, as shown in Fig. 2. In this paper, parameters of designed BE structures are chosen as following to efficiently excite surface plasmons. The period of grooves Λ for BE structures is equal to the wavelength λ of the designed THz source. The width of groove is set to be half the period. The depth of grooves h is equal to $\lambda/10$. The distance between the middle of the BE and the first groove C is set to be $5\lambda/2$.³⁷

The resonance frequency of bull's eye shaped plasmonic antenna can be adjusted using two different modes: groove-mode and cavity-mode (C-mode). Groove mode refers to adjusting the period of grooves, while the C-mode refers to optimizing the diameter of C value.

When the resonance frequency of grooves and C are the same, the plasmonic antenna achieves one single high transmission peak. To the contrary, when the resonance frequency of grooves and C are quite different, the transmission spectra of the plasmonic antenna will

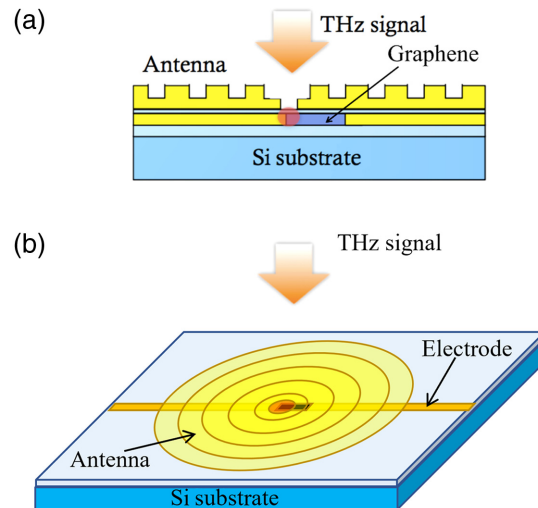


Fig. 1 (a) Cross-section structure and (b) bird-eye-view of the device design. The red point indicates the concentration of SPPs by the bull's eye antenna.

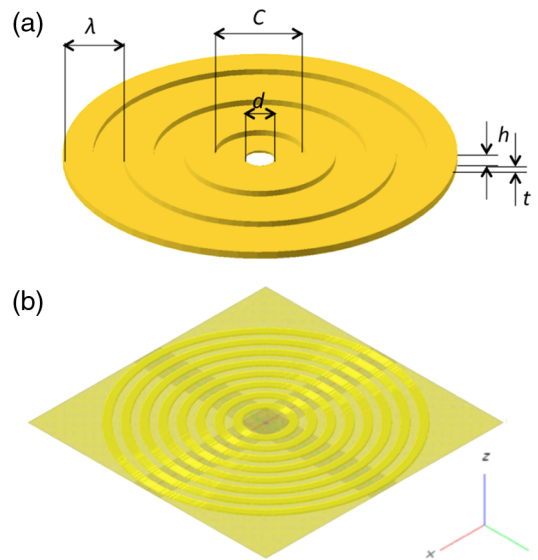


Fig. 2 (a) Schematic graph of the BE antenna. (b) Simulation model used in the FDTD software.

exhibit a much wider peak, which consists of the two peaks and results from the grooves and C , respectively. Figure 3 shows the change of transmission spectra for mid-infrared bull's eye structure when C varies from 18 to 30 μm . The resonance frequency of C peak grows larger from $C = 18 \mu\text{m}$ and reaches the highest value at $C = 27 \mu\text{m}$, then the transmission peak of the whole structure starts to become smaller. In addition, the resonance frequency reduces when C increases.

On the other hand, the excitation of surface plasmon polarizations strongly depends on the lattice constant of grooves, known as groove mode. The property of groove mode can be expressed by the following equation:

$$\beta = k \sin \theta \pm vg, \quad (1)$$

$$g = \frac{2\pi}{a}. \quad (2)$$

Here, g is the reciprocal vector of the grating, $v = (1, 2, 3, \dots)$, β is the propagation constant, θ is the angle under which photons impinging at the surface normal, and k is the wave vector.

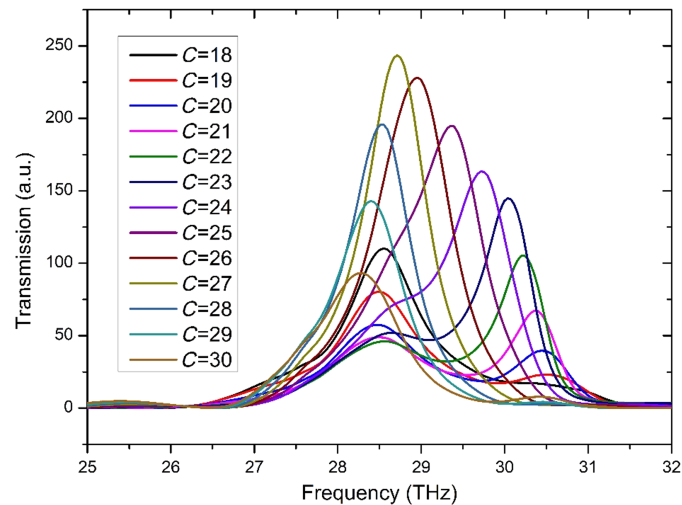


Fig. 3 Transmission comparison of different C value for mid-infrared bull's eye structure.

We designed two types of bull's eye antennas to fully cover the frequency range of our FIR laser. Optimized parameters of the two antennas are as follows. For the bull's eye structures with period λ at $10.25 \mu\text{m}$, height of grooves h is $1 \mu\text{m}$, thickness of metal is $0.2 \mu\text{m}$, diameter of the center aperture is set to be $5.125 \mu\text{m}$, and distance from the center of aperture to the first groove is $12.813 \mu\text{m}$. For the bull's eye structures with period λ at $9.5 \mu\text{m}$, height of grooves h is $1 \mu\text{m}$, thickness of metal is $0.2 \mu\text{m}$, diameter of the center aperture is set to be $4.75 \mu\text{m}$, and the distance from the center of aperture to the first groove is $13.3 \mu\text{m}$.

The transmission spectra in Fig. 4 indicated that both of the two designed antennas are wide-band comparing to conventional bull's eye antennas, and that the whole band width of the two bull's eye structures covers all of the effective frequencies of our FIR laser. High transmission enhancement appears at around 28 and 29.5 THz. Frequency that is out of this range, such as 32 and 33 THz does not show such high transmission enhancement. The wide-band FIR bull's eye structure we designed have a better opportunity to adapt the frequency of our laser and ensured the effectiveness of the bull's eye coupled Terahertz detection device. Thus, we select the wide-band bull's eye structure for fabrication and coupling with graphene ribbon.

3 Fabrication

Based on our simulation and device design, we fabricated our full-BE coupled graphene based midinfrared detectors according to the following procedures:

Low-resist Si wafer was selected as the substrate material. This will provide an easier gate modulation on the channel comparing to the high-resist ones. The Si wafer was cut into $1 \text{ cm} \times 1 \text{ cm}$ squares as Si substrate. Since graphene will be easier to observe when the thickness of SiO_2 is 90 or 300 nm, in order to ensure a smaller leakage current on the back-gate produced during ultrasonic bonding, we chose to fabricate an oxidation layer of 300 nm for this device. The CVD graphene was grown on copper foils and then transferred to the substrate. The location, shape, and quantity of the CVD graphene ribbon can be decided and designed. The graphene sheet on substrate is then designed using AutoCAD, patterned using EBL, and then etched using O_2 plasma. The length of graphene ribbon is designed to be $20 \mu\text{m}$. The width of graphene ribbon is $4.5 \mu\text{m}$. Negative resist is used during EBL in order to reduce the exposure time. Etching condition of O_2 plasma is room temperature, 50 W, and 10 s. After graphene patterning, electrodes are designed using AutoCAD and drawn using EBL. For the convenience of future device bonding, we designed one common electrode for every six devices. After development and rinse, the substrate is transferred to thermal deposition equipment for metal deposition. We chose Ni as the electrode material contacting the graphene ribbon. The thickness of Ni film deposited is 100 nm. Figure 5 displayed the fabricated graphene ribbon with electrodes and bonding pads under microscope. Figure 5(a) shows the overall structure of one set of devices (six devices). Figure 5(b) shows the detail figure of graphene ribbon with electrodes.

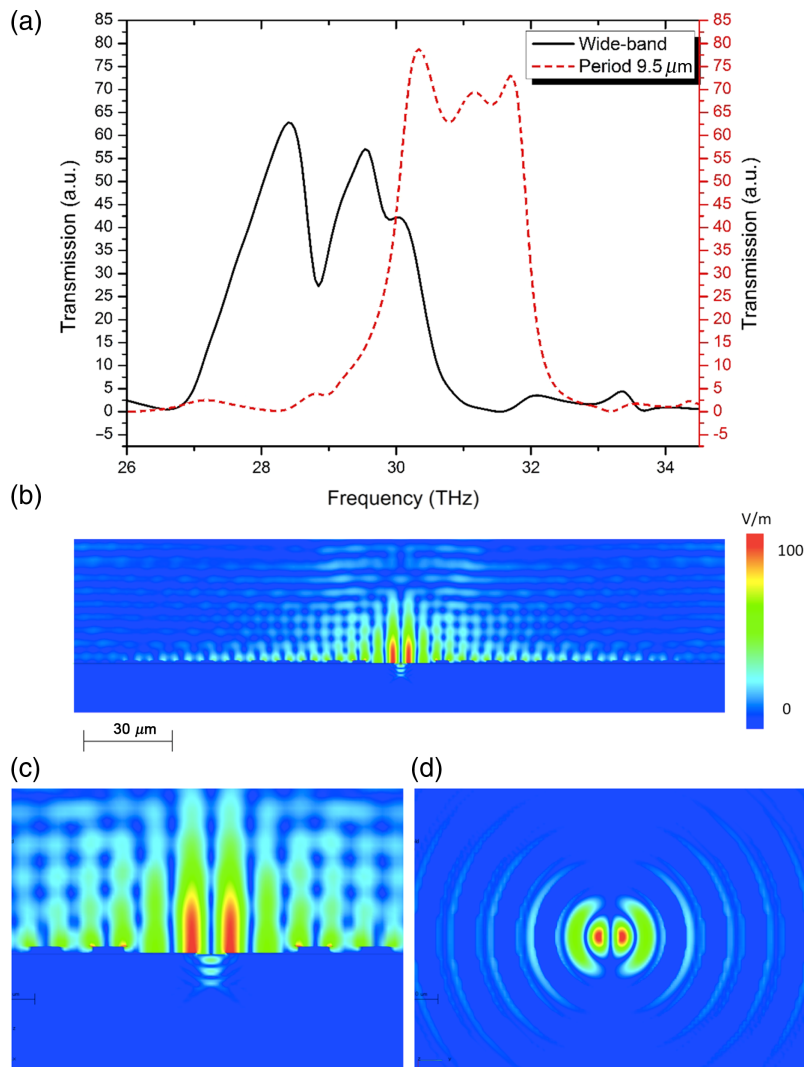


Fig. 4 (a) Transmission spectra of the two designed bull's eye plasmonic antennas. Black line represents the transmission spectrum of antenna structure with groove period of $10.25 \mu\text{m}$; red line represents the transmission spectrum of antenna structure with groove period of $9.5 \mu\text{m}$. (b)–(d) Electric field distribution of our multi-band bull's eye antenna. (b) Overall view and (c) magnified view of the electric field distribution on x - z plane. (d) Electric field distribution on x - y plane.

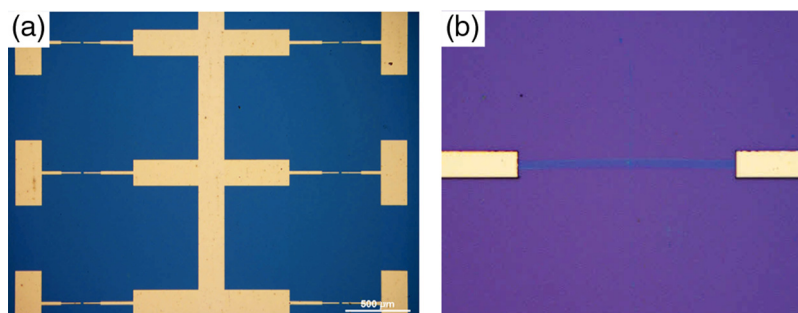


Fig. 5 (a) Electrode design. (b) Graphene ribbon with electrodes.

Bull's-eye-shaped plasmonic antennas are then designed and fabricated onto the graphene based devices. We first fabricated the metal plate for the bull's eye structure using EBL and thermal deposition, then we fabricated the grooves on top of the bull's eye structure using the same techniques. Figure 6 exhibits the fabricated device. Figure 6(b) shows the microscopic image of the bull's eye structure.

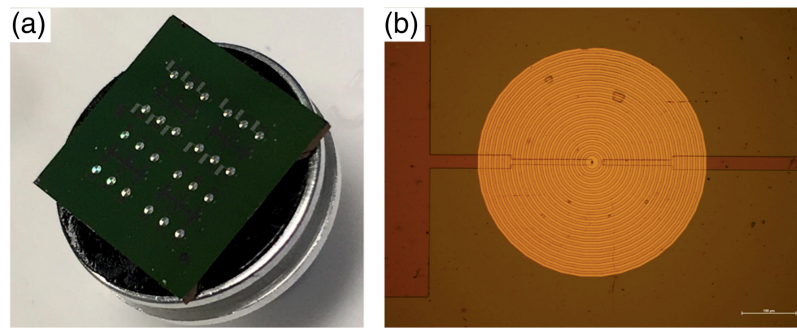


Fig. 6 (a) Photo of the fabricated device. (b) Microscopic image of the fabricated device.

4 Measurements and Results Analysis

Before measuring the electric properties and midinfrared response of our fabricated devices, we conducted several observation and measurement to confirm the existence (after such complicated fabrication process) and quality of the CVD graphene ribbon. We first observed the device under SEM. Figure 7 displayed the SEM photo captured at the aperture of bull's eye structure. The graphene ribbon clearly appears in the middle of the aperture.

To verify the quality of the graphene ribbon, we conducted Raman measurement in and around the aperture. Figure 8(a) shows the Raman spectroscopy of the graphene ribbon, d , g , and $2d$ peaks are clearly shown at the graphene ribbon, indicating a good quality of our monolayer graphene ribbon. We have also done a Raman mapping around the aperture. The results are mapped out in Figs. 8(b)–8(d). We can observe in Fig. 8(b) clearly the existence and location of the graphene ribbon.

We then cut and bond the full-BE coupled graphene devices onto chip carriers using ultrasonic bonding machine and measured their electrical properties using precision semiconductor parameter analyzer. Figure 9 exhibits the I_d - V_g characteristic of our CVD graphene based device. The Dirac point appears at around -0.7 V, which is much smaller than that of our previous device. This indicates a good gate modulation of the fabricated device.

Figure 10 presents the IR reflection spectrum measured with FTIR. The experimental data correspond well with the simulation results, with absorption peaks appear at around 28.5 and 29.5 THz, where transmission is relatively higher. The high consistency between our numerical simulation results and the spectrum measurement of our complete device with graphene ribbon also proved that the existence of the monolayer graphene ribbon does not affect the transmission spectra at 28.5 and 29.5 THz of the proposed bull's eye plasmonic antenna. The electrode used to connect the graphene split the BE into two halves, which caused the new spectrum at 31.5 THz.

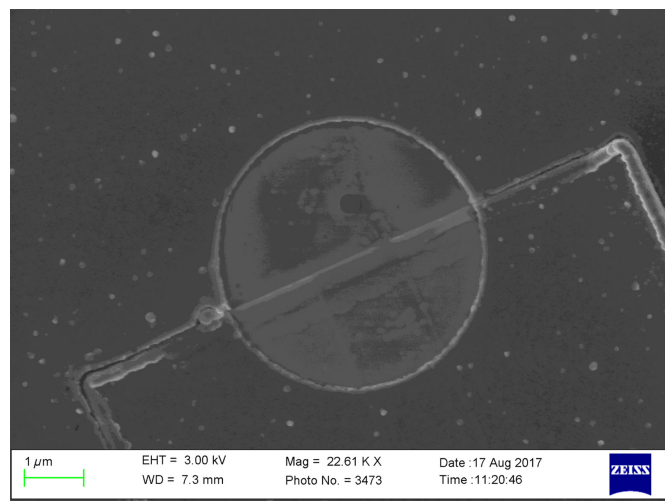


Fig. 7 SEM image around the aperture. Graphene ribbon is clearly observed in the aperture.

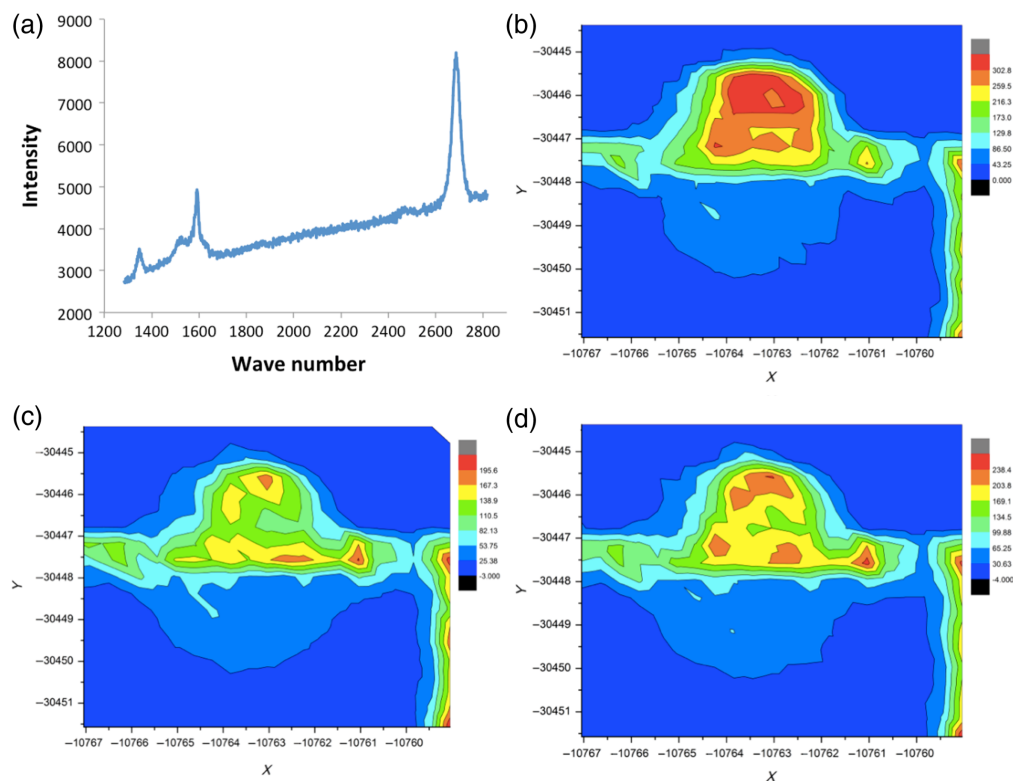


Fig. 8 (a) Raman spectroscopy of the graphene ribbon. (b) Raman mapping of the $2d$ peak. (c) Raman mapping of the d' peak. (d) Raman mapping of the g peak.

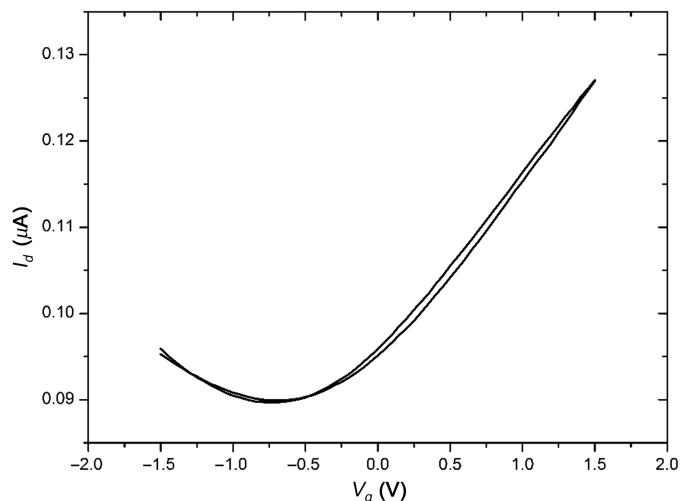


Fig. 9 I_d - V_g characteristic of CVD monolayer graphene based device. The gate voltage is double swept from -1.5 V to 1.5 V.

This phenomenon was also observed in our previous study with half-BE coupled graphene device,³¹ where we also observed additional spectrum at 31.4 THz with half-BE.

We then irradiated midinfrared signal from FIR laser to the device and measured its mid-infrared response. We used the lock-in amplifier to reduce the noise and filter out the signal. We first measured the relation between photocurrent and drain voltage. Figure 11 shows our measured result. The result exhibits larger response upon higher drain voltage. But the response seems to be more stable when drain voltage is smaller than 20 mV. In this case, we set the drain voltage to be 10 mV for our next measurement. We then measured the relation between

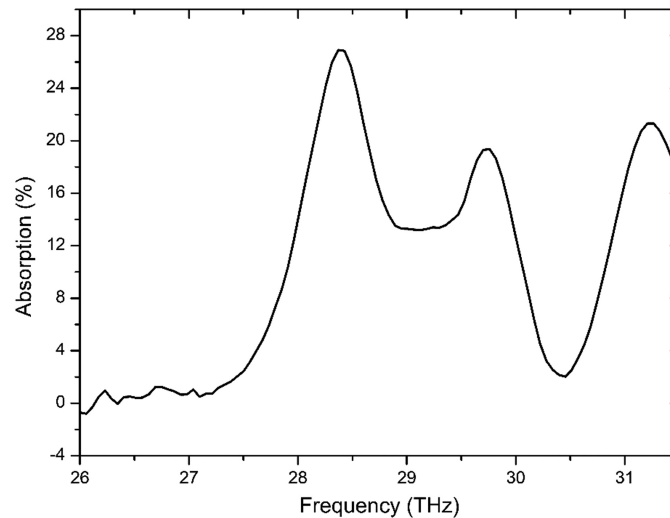


Fig. 10 IR absorption spectrum of double-resonance frequency bull's eye structure measured on FTIR. Absorption rate peak appears at around 28.5, 29.5, and 31.4 THz.

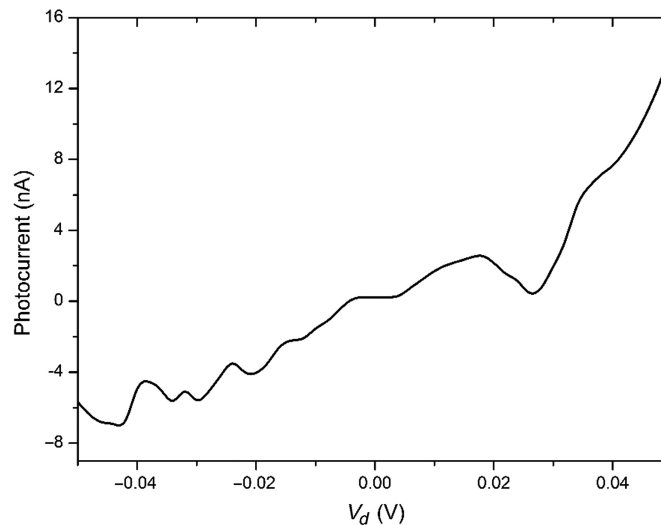


Fig. 11 Photocurrent versus drain voltage characteristics upon 31.4 THz signal. The photocurrent is acquired through lock-in amplifier.

photocurrent and gate voltage. Drain voltage is set to 10 mV. The results are displayed in Fig. 12. For the full-BE coupled graphene based devices, the result exhibits a highest photocurrent at around Dirac point of $V_g = -0.7$ V, which indicated a responsivity of $29.8 \mu\text{A}/\text{W}$. The repeat experiment of photocurrent measurement at Dirac point shows no degradation of over 20 measurement cycles, proving the good stability of the proposed photodetector. The appearance of photocurrent is due to Seebeck effect, which is induced by the thermal gradient between the two electrodes connecting the graphene ribbon. The Seebeck coefficient is highest near the Dirac point for the graphene nanoribbon,³⁸ which explains the highest photocurrent at $V_g = -0.7$ V. In addition, in Seebeck effect, the generated photocurrent is proportional to the thermal gradient. It is also shown in study that photo response is stronger upon higher incident light intensity, whereas weaker photo response upon lower incident light intensity.³⁹ The frequency selective characteristic of bull's eye antenna filters out the non-objected frequencies other than those at transmission spectrum peaks. As studied in one of our previous works, the insufficient E -field concentration and transmission for the non-objected frequencies at the BE aperture cannot generate adequate thermal gradient on the graphene ribbon, resulting in zero photocurrent.³¹

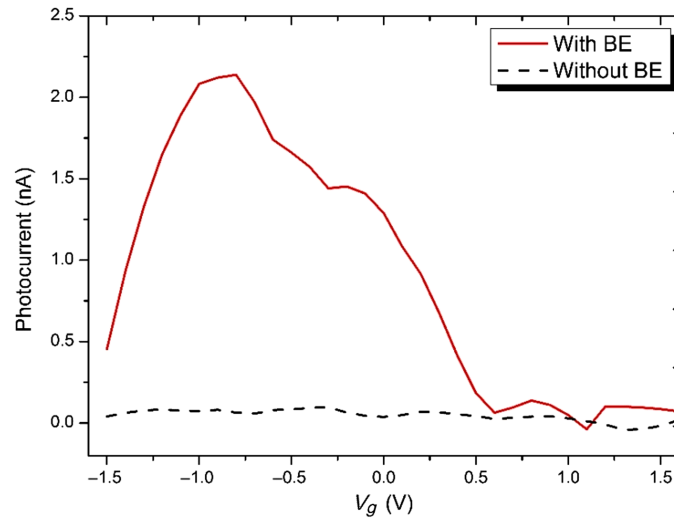


Fig. 12 Photocurrent versus gate voltage upon 31.4 THz signal. The photocurrent is acquired through lock-in amplifier. Red line represents the measurement results of graphene based devices with bull's eye plasmonic antenna, while the black line represents the measurement results of only graphene ribbon with electrodes.

Table 1 Comparison of our device performance with other works using different antennas.

Antenna type	R_A (A/W)	R_v (V/W)	D^* (cm $\sqrt{\text{Hz/W}}$)	Frequency selectivity
Full-BE (this work)	178×10^{-6}	19.31	1.63×10^7	○
Crystal substrate (Gopalan et al.) ⁴¹	—	—	1.14×10^5	×
End to end coupled antenna (Yao et al.) ²⁶	—	0.4	—	×
Dipole array (Long et al.) ⁴²	34×10^{-6}	—	—	×
Log periodic antenna (Vicarelli et al.) ⁴⁰	—	0.15	—	×

$$\text{NEP} = \frac{N}{R_v} = \frac{\sqrt{4k_BRT}}{R_v}. \quad (3)$$

Largest responsivity can be achieved at $V_d = 0.05$ V, leading to a responsivity of $178 \mu\text{A/W}$ (19.31 V/W); the NEP of our full-BE coupled graphene-based detector is estimated according to Eq. (3), obtaining 2.17 nW/ $\sqrt{\text{Hz}}$; the D^* is estimated accordingly, obtaining 1.63×10^7 cm $\sqrt{\text{Hz/W}}$, which is superior to the recently reported graphene-based mid-infrared detectors.^{26,40–42} We have also fabricated some graphene ribbons without bull's eye antennas for comparison. These devices did not show obvious response upon midinfrared irradiation.

Table 1 also listed the comparison results with other works using graphene as the active material, but with different antenna coupling. It confirms that the performance of our bull's eye coupled graphene-based device is superior to other related works.

5 Summary

In conclusion, we designed and fabricated the full-bull's eye coupled graphene based detector. The graphene we used in this device is CVD grown monolayer graphene. The fabricated device exhibits a responsivity of $178 \mu\text{A/W}$. The device can be operated in non-vacuum condition and room temperature. The nature of CVD grown graphene makes it easy for us to decide the shape, size, location, and quantity of the graphene ribbons, which further reduce the fabrication expense and allows for large amount integration in the future. We believe that such a device will have

potential applications in various fields that require frequency selective, room-temperature sensitive photo detection.

Data Availability Statement

The authors confirm that the data supporting the findings of this study are available within the article.

Acknowledgments

This work was supported by the Engineering Schools International Exchange program and Support for Tokyo Tech Advanced Researchers (STAR), the Mirai Program of the Japan Science and Technology Agency, JSPS KAKENHI of the Japan Society for the Promotion of Science (JP21H01746, JP21H05809, JP22H01553, JP22H01555, JP22H05470, and JP23H00169), and Strategic Research Development Program of the Kanagawa Institute of Industrial Science and Technology. We acknowledge technical support from Research Centre on Graphene, Layered Crystals and Hybrid Nanomaterials of University of Cambridge.

References

1. S. Lukman et al., "High oscillator strength interlayer excitons in two-dimensional heterostructures for mid-infrared photodetection," *Nat. Nanotechnol.* **15**, 675–682 (2020).
2. E. Wu et al., "In situ fabrication of 2D WS₂/Si type-II heterojunction for self-powered broadband photodetector with response up to mid-infrared," *ACS Photonics* **6**(2), 565–572 (2019).
3. C. You et al., "Design and performance study of hybrid graphene/HgCdTe mid-infrared photodetector," *IEEE Sens. J.* **21**(23), 26708–26715 (2021).
4. M. Ye et al., "Graphene-based mid-infrared photodetectors using metamaterials and related concepts," *Appl. Phys. Rev.* **8**, 031303 (2021).
5. J. Bai et al., "Graphene nanomesh," *Nat. Nanotechnol.* **5**, 190–194 (2010).
6. F. Jabbarzadeh et al., "Modification of graphene oxide for applying as mid-infrared photodetector," *Appl. Phys. B* **120**, 637–643 (2015).
7. X. Yu et al., "Narrow bandgap oxide nanoparticles coupled with graphene for high performance mid-infrared photodetection," *Nat. Commun.* **9**, 4299 (2018).
8. D. Basko, "A photo thermoelectric effect in graphene," *Science* **334**, 610–611 (2011).
9. T. Mueller, F. Xia, and P. Avouris, "Graphene photodetectors for high-speed optical communications," *Nat. Photonics* **4**, 297–301 (2010).
10. X. Cai et al., "Sensitive room-temperature terahertz detection via the photothermoelectric effect in graphene," *Nat. Nanotechnol.* **9**, 814–819 (2014).
11. J. Liu et al., "Semimetals for high-performance photodetection," *Nat. Mater.* **19**, 830 (2020).
12. K. J. A. Ooi et al., "Nonlinear plasmonics of three-dimensional Dirac semimetals," *APL Photonics* **4**, 034402 (2019).
13. J. Lim et al., "Efficient generation of extreme terahertz harmonics in three-dimensional Dirac semimetals," *Phys. Rev. Res.* **2**, 043252 (2020).
14. H. Meng et al., "Terahertz polarization conversion from optical dichroism in a topological Dirac semimetal," *Appl. Phys. Lett.* **121**, 193102 (2022).
15. T. J. Echtermeyer et al., "Surface plasmon polariton graphene photodetectors," *Nano Lett.* **16**, 8–20 (2015).
16. H. Chang et al., "Facile synthesis of wide-bandgap fluorinated graphene semiconductors," *Chem. Eur. J.* **17**(32), 8896–8903 (2011).
17. H. Chang et al., "Thin film field-effect phototransistors from bandgap-tunable, solution-processed, few-layer reduced graphene oxide films," *Adv. Mater.* **22**(43), 4872–4876 (2010).
18. H. Yan et al., "Infrared spectroscopy of wafer-scale graphene," *ACS Nano* **5**(12), 9854–9860 (2011).
19. B. Chitara et al., "Infrared photodetectors based on reduced graphene oxide and graphene nanoribbons," *Adv. Mater.* **23**(45), 5419–5424 (2011).
20. M. Furchi et al., "Microcavity-integrated graphene photodetector," *Nano Lett.* **12**(6), 2773–2777 (2012).
21. B. Nie et al., "Monolayer graphene film on ZnO nanorod array for high-performance Schottky junction ultraviolet photodetectors," *Nanotechnology* **9**(17), 2872–2879 (2013).
22. Z. Qu et al., "Waveguide integrated graphene mid-infrared photodetector," *Proc. SPIE* **10537**, 105371N (2018).
23. X. Deng et al., "Terahertz plasmonics and nano-carbon electronics for nano-micro sensing and imaging," *Int. J. Autom. Technol.* **12**(1), 87–96, (2018).

24. Z. Sun et al., "Infrared photodetectors based on CVD-grown graphene and PbS quantum dots with ultrahigh responsivity," *Adv. Mater.* **24**, 5878–5883 (2012).
25. Z. Fang et al., "Plasmon-induced doping of graphene," *ACS Nano* **6**(11), 10222–10228 (2012).
26. Y. Yao et al., "High-responsivity mid-infrared graphene detectors with antenna-enhanced photocarrier generation and collection," *Nano Lett.* **14**(7), 3749–3754 (2014).
27. J. J. Wood et al., "Spoof plasmon polaritons in slanted geometries," *Phys. Rev. B* **85**, 075441 (2012).
28. X. Deng et al., "Continuously frequency-tuneable plasmonic structures for terahertz bio-sensing and spectroscopy," *Sci. Rep.* **9**(1), 3498, (2019).
29. S. Liu, X. Shou, and A. Nahata, "Coherent detection of multiband terahertz radiation using a surface plasmon-polariton based photoconductive antenna," *IEEE Trans. Terahertz Sci. Technol.* **1**, 412 (2011).
30. D. S. Bulgarevich, M. Watanabe, and M. Shiwa, "Single sub-wavelength aperture with greatly enhanced transmission," *New J. Phys.* **14**, 053001 (2012).
31. X. Deng et al., "Surface plasmon polariton graphene midinfrared photodetector with multifrequency resonance," *J. Nanophotonics* **12**(2), 026017 (2018).
32. O. Mahboub et al., "Optimization of bull's eye structures for transmission enhancement," *Opt. Express* **18**, 11292 (2010).
33. D. Wang, T. Yang, and K. B. Crozier, "Optical antennas integrated with concentric ring gratings: electric field enhancement and directional radiation," *Opt. Express* **19**, 2148 (2011).
34. F. Ren et al., "Second-order surface-plasmon assisted responsivity enhancement in germanium nanophotodetectors with bull's eye antennas," *Opt. Express* **22**, 15949 (2014).
35. M. Yang et al., "Split bull's eye antenna for high-speed photodetector in the range of visible to mid-infrared," *IEEE Photonics Technol. Lett.* **28**, 1177 (2016).
36. T. Iguchi, T. Sugaya, and Y. Kawano, "Silicon-immersed terahertz plasmonic structures," *Appl. Phys. Lett.* **110**, 151105 (2017).
37. X. Deng et al., "Frequency selective, high transmission spiral terahertz plasmonic antennas," *J. Model. Simul. Antennas Propag.* **2**, 1–6 (2016).
38. Y. Xing, Q. Sun, and J. Wang, "Nernst and Seebeck effects in a graphene nanoribbon," *Phys. Rev. B* **80**, 235411 (2009).
39. D. Suzuki, S. Oda, and Y. Kawano, "A flexible and wearable terahertz scanner," *Nat. Photonics* **10**, 809–813 (2016).
40. L. Vicarelli et al., "Graphene field-effect transistors as room-temperature terahertz detectors," *Nat. Mater.* **11**, 865–871 (2012).
41. K. K. Gopalan et al., "Mid-infrared pyroresistive graphene detector on LiNbO₃," *Adv. Opt. Mater.* **5**(4), 1600723 (2017).
42. L. Xiao et al., "High responsivity detection of terahertz quantum cascade lasers with graphene-loaded plasmonic antenna arrays," in *Int. Conf. Intersubband Transit. in Quantum Wells*, Singapore (2017).

Xiangying Deng is a staff engineer at Western Digital Technologies Inc. She received her BS degree from Jilin University in 2012, and her MS degree in physics from Temple University in 2014, and his PhD in physical electronics from Tokyo Institute of Technology in 2018. Her research interests include photodetectors in terahertz and midinfrared spectra region.

Shunri Oda received his PhD from Tokyo Institute of Technology in 1979. He is a professor in the Department of Physical Electronics and Quantum Nanoelectronics Research Center, Tokyo Institute of Technology. His research interests include fabrication of silicon quantum dots, single-electron tunneling devices, ballistic transport in silicon nanodevices, and NEMS hybrid devices. He is a fellow of the Institute of Electrical and Electronics Engineers (IEEE) and a distinguished lecturer at the IEEE Electron Device Society.

Yukio Kawano received his PhD from the University of Tokyo, Japan, in 2001. From 2011 to 2021, he was an associate professor in the Laboratory for Future Interdisciplinary Research of Science and Technology at the Tokyo Institute of Technology, Japan. Since 2021, he has been working as a professor in the Faculty of Science and Engineering at Chuo University, Japan. His research interests include terahertz engineering, image sensing, and material science.